Oxygen ion irradiation of tholins: Implications for the incorporation of oxygen into aerosols in Titan's atmosphere

Filip Matuszewski, Véronique Vuitton, Lionel Vacher, Laurène Flandinet, Lydie Bonal, P. Boduch, Alicja Domaracka, Hermann Rothard, Sarah M. Hörst, Cara Pesciotta, et al.

Draft version November 24, 2025
Typeset using LaTeX **preprint** style in AASTeX7.0.1

Oxygen ion irradiation of tholins: Implications for the incorporation of oxygen into aerosols in Titan's atmosphere

Filip Matuszewski [1], Véronique Vuitton [1], Lionel Vacher [1], Laurène Flandinet [1], Lydie Bonal [1], Philippe Boduch [2], Alicja Domaracka [2], Hermann Rothard [2], Sarah M. Hörst [3], Cara Pesciotta [3] and Chao He [4]

[1] *Univ. Grenoble Alpes, CNRS, IPAG, Grenoble, 38000, France*
[2] *Centre de Recherche sur les Ions, les Matériaux et la Photonique CIMAP Normandie Univ, ENSICAEN, UNICAEN, CEA, CNRS, 14000, Caen, France*
[3] *Johns Hopkins University, Department of Earth and Planetary Science, Baltimore, MD 21218, USA*
[4] *School of Earth and Space Sciences, University of Science and Technology of China, Hefei, Anhui, China*

ABSTRACT

Heavy molecules reaching several thousand atomic mass units and O^+-ions have been detected in Titan's atmosphere and magnetosphere, respectively. The heavy molecules are attributed to potentially nitrogenous polycyclic aromatic hydrocarbons (PANH) while the energetic O^+-ions deposit in Titan's upper atmosphere and may be expected to alter the structure and chemical composition of these macromolecules by implantation and incorporation. This process was studied by irradiating thin-film tholin samples with either $^{18}O^{q+}$ or $^{20}Ne^{q+}$ ions at different energies (35 and 70 keV), temperatures (150 and 300 K), and fluences ($0.6 - 4 \times 10^{15}$ ions.cm^{-2}). Ex-situ elemental analysis isotope ratio mass spectrometry (EA-IRMS) was used to determine the stable oxygen isotope composition of both the soluble and insoluble fractions of the irradiated samples, assessing ion-induced oxygen incorporation. The results demonstrate a significant increase in ^{18}O for all samples irradiated with O ions, whereas non-irradiated and Ne-irradiated samples show no such enhancement. This confirms that oxygen implantation into tholins is possible. The fraction of incident oxygen ions incorporated into the tholins ranges from approximately 2-16%, depending on sample properties, solubility fractions, and film thickness. These findings provide important insights into the role of energetic oxygen species in modifying Titan's organic aerosols. The incorporation of oxygen has implications for the formation of oxygenated molecules with astrobiological interest.

Keywords: Tholins — keV ion irradiation — Isotope ratio mass spectrometry — Titan atmosphere — oxygen implantation

1. INTRODUCTION

In its 13 years of operation, the Cassini-Huygens mission revealed a complex chemical diversity on Saturn's moons Titan and Enceladus. Two discoveries are of particular interest for this study.

Email: matuszewskifil@gmail.com

First, positively and negatively charged ions with masses reaching up to thousands of atomic mass units were detected in Titan's atmosphere (J. H. Waite et al. 2007; F. J. Crary et al. 2009). These macromolecules are the precursors of the aerosols known to be present at lower altitude creating Titan's haze (P. Lavvas et al. 2013) and are attributed to potentially nitrogenous polycyclic aromatic hydrocarbons (M. López-Puertas et al. 2013; R. P. Haythornthwaite et al. 2021). They are formed through photochemistry, initiated by UV-radiation of N_2 and CH_4. The second discovery, positively charged oxygen ions have been observed in Saturn's magnetosphere, most likely originating from cryovolcanism on Enceladus (R. Johnson et al. 2005; E. Sittler Jr et al. 2006). These, oxygen ions deposit in Titan's atmosphere between 1200 and 800 km, providing up to 10^6 ions.cm^{-2} s^{-1} (R. E. Hartle et al. 2006a,b; D. Snowden et al. 2018). As these ions enter Titan's atmosphere, energy is lost through both electronic excitation and momentum transfer to the ambient molecules, primarily N_2 (T. E. Cravens et al. 2008). They posses energies between 1 and 100 keV. S. M. Hörst et al. (2008) suggested that the influx of these oxygen ions provides a crucial source of oxygen, leading to the formation of CO and CO_2. This rules out the possibility of these species being primordial remnants and highlights the importance of energetic oxygen ions in the oxygen chemistry of Titan's atmosphere. Furthermore, it has been proposed that during the descent into Titan's atmosphere, O^+-ions could be implanted into the complex organic molecules of the atmospheric haze, creating oxygenated species and possibly molecules like amino acids and nucleic bases with strong astrobiological implications (E. Sittler Jr et al. 2009; E. C. Sittler et al. 2020). The chemical interactions between energetic ions and these macromolecules are poorly understood and are therefore worthy of simulation in a laboratory environment.

Previous studies have investigated sulfur ion implantation into astrophysical ice analogs composed of H_2O, CO, CO_2, or O_2 (G. Strazzulla et al. 2007; J. Ding et al. 2013; X. Lv et al. 2014; P. Boduch et al. 2016; D. V. Mifsud et al. 2024). These studies demonstrated that sulfur ions can be incorporated into these compounds, leading to the formation of sulfur-containing compounds, e.g.: hydrated sulfuric acid and sulfides like CS_2 and OCS. Building on this work, A. Ruf et al. (2019) conducted a similar experiment in which they irradiated an ice mixture of H_2O:CH_3OH:NH_3 in a 2:1:1 ratio with 105 keV S^{7+} ions. Their results revealed the formation of more than 1100 distinct organosulfur (CHNOS) molecules, highlighting the efficiency of ion implantation into organics in astrophysical environments. Compared to sulfur ion implantation, significantly less research has been conducted on the implantation of oxygen ions. E. Sittler Jr et al. (2009) proposed that energetic oxygen ions could become incorporated into complex molecules in Titan's atmosphere, using fullerenes as a potential example. Additionally, in the context of material science, G. Xu et al. (2000) have demonstrated that keV oxygen ions can be incorporated into polysulfones, where they chemically bind in the form of hydroxyl and carboxyl functional groups. Similar processes may occur in the complex organic environments on Titan.

The aerosols in Titan's atmosphere are significantly more complex consisting of a plethora of different organic molecules. Tholins are the laboratory analogs of these aerosols and have been extensively investigated to illuminate chemical processes on Titan (M. L. Cable et al. 2012). L. Jovanovic (2021) irradiated tholin with heavy high-energy ions ($^{58}Ni^{q+}$ 33.64 MeV and $^{136}Xe^{q+}$ 74.8 MeV), causing changes in their chemical composition. The tholin in this experiment simulate Pluto, starting with an initial gas mixture of N_2, CH_4, and CO, producing polyaromatic nitrogen-bearing hydrocarbons containing oxygen. This suggests a chemical rearrangement of existing oxygen atoms in the tholins.

Studies concerning the effect of oxygen ion irradiation on tholins have not been made. In this study, we investigate the effect of irradiating tholin thin films with low energy (30-70 keV) $^{18}O^{q+}$- and $^{20}Ne^{q+}$-ions. Elemental analysis for isotope ratio mass spectrometry (EA-IRMS) of the insoluble and soluble part of these irradiated tholins determines the degree of oxygenation and check whether an ion-induced incorporation process of ^{18}O would be possible.

2. METHODS

The methods in this work are organized in three parts, where at first, Titan aerosol analogs or tholins are synthesized. Following this, the irradiation experiment is described in detail, ending with the last part of ex-situ isotope ratio mass spectrometry.

2.1. *Sample synthesis*

The tholin samples were prepared at John Hopkins University (JHU) utilizing the PHAZER (Planetary HAZE Research) chamber, which is described in detail in C. He et al. (2017, 2022). Here, an initial gas mixture of 97.44% CH_4 and 2.56% N_2 (initial aim at 97.5%:2.5%) was subjected to a cold plasma discharge. The flow rate of the gas mixture was kept at 5.01 sccm, resulting in a chamber pressure of 2.5 torr. Inside the chamber, 14 round windows made of MgF_2 with a 2 cm diameter and 2 mm thickness were placed. The experiment lasted approximately 43 hours, coating the entire chamber and windows surface with a thin film of ∼500 nm thickness. This thickness was chosen in order to maximize the chances of ion implantation into the tholin sample. The goal was to ensure that the projected range (penetration depth) of the ion was smaller than the sample's thickness. This ideally ensures that the ions remain in the sample and not pars through it, implanting into the MgF_2 window, instead. A common method to determine this projected range is using the "The Stopping and Range of Ions in Matter" (SRIM) software developed by J. F. Ziegler et al. (2010). This software, however, uses a single compound as the to-be bombarded material, which is not the case for a complex mixture of organics like tholins. We can approximate the tholins in this simulation using an organic analogue material that is rich in nitrogen. In this case, we chose adenine to calculate the approximate projected ranges with SRIM, which fell below 500 nm, independent of the energies used in our experiments. After collecting the windows from the chamber, they were placed in a desiccator filled with pure nitrogen gas to minimize contamination with ambient air until the following experiments. Tholins that coated the inner walls of the chamber were scraped off and placed in a separate container serving as "powder sample".

2.2. *Irradiation experiments*

The irradiation experiments were carried out at the Grand Accélérateur National d'Ions Lourds (GANIL) in Caen, France. The "Accélérateur pour la Recherche avec des Ions de Basse Energie" (ARIBE) platform was used in conjunction with the "Irradiation de GLaces d'Intérêt Astrophysique" set-up (IGLIAS), as outlined by B. Augé et al. (2018). A total of 12 tholin thin-film samples were subjected to $^{18}O^{q+}$- and $^{20}Ne^{q+}$-ion beams with energies of either 35 or 70 keV. The maximum total fluence ranged between 0.6 and 4×10^{15} ions.cm^{-2}. The IGLIAS set-up allows the sample holder to be cooled down, which was done for half of the samples to 150 K to mimic the conditions in Titan's upper atmosphere (S. M. Hörst 2017). The other half of the samples were kept at ∼300 K to have a room temperature comparison. This was done because, despite achieving an ultra-high vacuum down to 8×10^{-9} mbar, the possibility of water-vapor condensing to ice inside the chamber

at low temperatures existed. Of the two remaining thin-film samples, one was not used in the irradiation experiments, while the other was kept in the sample holder of the experimental chamber at all time without being irradiated itself (T0f). These serve as blank controls for the subsequent chemical analysis. Table 1 shows the sample names together with the experimental free parameters mentioned above. Given the limited number of samples, the large number of free parameters may appear unconventional. However, the experimental conditions were intentionally varied extensively in order to maximize the chance of ion incorporation. After the experiment was completed, it was found that the ion beam was misaligned with the target, leading to an overestimation of the number of ions reaching the target. Figure 1 shows a photograph of the sample holder with a sample unrelated to this study that was irradiated right before our experiments. Here, the "shadow" left by the ion beam does not completely cover the target area. Due to this misalignment the number of projectiles that reached the samples does not correspond to the indicated fluence values, but was about 30% lower than expected. This error is the same for all irradiated samples. While this does not impact the relative trends of the results as a function of fluence, it introduces a greater uncertainty in the determination of the fraction of ions implanted into the sample from the ion beam.

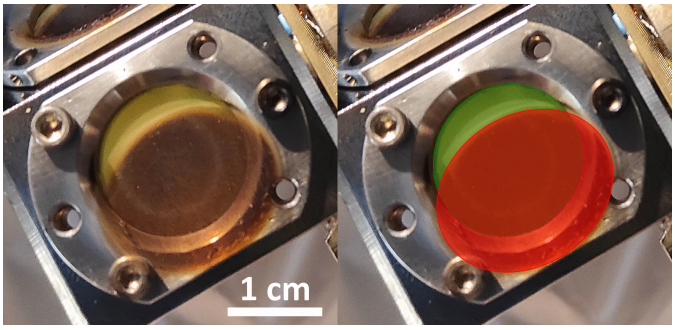

Figure 1. Photograph of the sample holder and the target (green) with the darker shadow indicating ion irradiated surface (red). Due to the misalignment of the ion beam about 30% of the sample was not irradiated.

2.3. *Sample dissolution and preparation for analysis*

Because it was not possible to scrape off enough material from the sample windows for conventional EA-IRMS analysis, the thin films were first solubilized to detach the tholins from the windows prior to analysis. Tholins are composed of a soluble and insoluble part which differ in their chemical composition (Á. Somogyi et al. 2012; J. Maillard et al. 2018; F. Schulz et al. 2021). The solubilization process allowed us to separate and analyze both these fractions of the sample. This distinction provides additional insight into the chemical composition and structural properties of the material. Every thin-film window was submerged in 4 ml of methanol (CH_3OH, Carlo Erba $\geq$ 99.99 %) and left overnight. For the powder sample (T0p), 1 mg of powder was used instead, while the rest of the procedure remained unchanged. A 20-minute ultrasonic bath ensured a nearly complete detachment of the tholins from the windows. Only a very small amount of residue on the windows remained. Centrifuging the solutions for 15 minutes at 4000 rpm ensured the precipitation of the insoluble components to the bottom of the sample flask. The insoluble parts of the samples were transferred into silver capsules (Elemental Microanalysis, D2003) by collecting $\sim$30 μL from the bottom of the sample flask using a pipette. The capsules were left for about 30 min for the solvent to evaporate. This was repeated up to 3 times to ensure that the weight was in the range of $>$250 μg. While this approach

Table 1. List of tholin samples together with free experimental parameters

Sample		Energy	Temperature	max. Fluence	Sample weight [μg]	
name	Ion	[keV]	[K]	[$\times 10^{15}$ ions.cm^{-2}]	insoluble	soluble
T0p	non-irradiated				112±6	230±12
T0f					155±8	270±14
T1	$^{18}O^{3+}$	35	150	1	215±11	270±14
T2	$^{18}O^{3+}$	35	150	1	283±14	260±13
T3	$^{18}O^{3+}$	35	300	0.6	291±15	250±13
T4	$^{18}O^{3+}$	35	300	1	264±13	240±12
T5	$^{18}O^{5+}$	70	300	4	307±15	250±13
T6	$^{18}O^{5+}$	70	300	2	212±11	320±16
T7	$^{18}O^{5+}$	70	150	1	351±18	260±13
T8	$^{18}O^{5+}$	70	150	1	229±11	260±13
T9	$^{20}Ne^{3+}$	35	300	1	485±24	220±11
T10	$^{20}Ne^{3+}$	35	150	1	197±10	260±13
T11	$^{20}Ne^{6+}$	70	300	1	219±11	220±11
T12	$^{20}Ne^{6+}$	70	150	1	280±14	260±13

is effective in extracting the insoluble compounds from the sample, some of the soluble fraction is inadvertently captured in the capsules. For the preparation of the soluble phase, a similar evaporation process was employed. However, instead of silver capsules, silver boats (Elemental Microanalysis, D5008) were used due to their larger volume for faster solvent evaporation. The oxygen blank signal was ten times higher for these larger silver boats than that of the silver capsules, directly affecting the detection limit. Therefore, a rigorous cleaning procedure was implemented which can be found in the supplementary material. As the soluble phase contained significantly less material than the insoluble fraction, a greater number of evaporation steps (up to 18) was necessary to accumulate a sufficient sample mass for analysis. The sample boats were kept covered under a fume hood for two days to allow the solvent to evaporate. However, since we could not verify whether all solvent had been completely removed, there may be a bias in the weight measurements due to residual solvent, introducing an uncertainty that we cannot accurately estimate. Hence, the uncertainties in table 1 refer to the 5% instrumental error of the high-precision balance.

2.4. *EA-IRMS*

The total oxygen abundance (wt% (O)) and isotopic composition expressed as,

$$\delta^{18}O = \left[\frac{\left(\frac{^{18}O}{^{16}O}\right)_{sample}}{\left(\frac{^{18}O}{^{16}O}\right)_{VSMOW}} - 1 \right] \times 1000, \quad (1)$$

relative to VSMOW = Vienna Standard Mean Ocean Water) of the tholins were determined using the Thermo Scientific Elemental Analyzer (EA) IsoLink deltaV Isotope Ratio Mass Spectrometer (IRMS) System at the Institut de Planétologie et d'Astrophysique de Grenoble (IPAG, France). The capsules were placed into a custom sealed, auto-sampler pre-flushed with helium (He) to limit the contribution of the N_2 and CO blank on oxygen isotopic data. The autosampler was then connected to the EA, evacuated for 10 minutes, and filled with He. This purging procedure was repeated several times before the autosampler was opened to the reduction column. The samples pyrolysis was performed at 1450 °C on an EA glassy carbon reaction tube filled with glassy carbon chips and enclosed into a ceramic liner to convert oxygen released by the samples into CO. The He carrier gas flow was set to 100 mL/min, and the chromatographic separation was maintained at 50 °C to ensure sufficient peak separation between CO and N_2 released during the pyrolysis of nitrogen-rich tholins. A dilution procedure was applied before detecting the CO peak to reduce the N_2 signal reaching the detectors and to minimize the mass 28 interference from N_2 on CO. Additionally, a partial-peak integration procedure was used to minimize any residual N_2 tailing on CO, in which only 50% of the central CO peak area was retained. A figure illustrating this peak integration can be found in the supplementary material. Oxygen isotope compositions were calibrated using three reference materials over three different analytical sessions: B2203 (EMA-P1, $\delta^{18}O$ = 21.0 ± 0.7 ‰, 1σ, Elemental Microanalysis) and IAEA-NBS18 (Calcite, $\delta^{18}O$ = 7.0 ± 0.1 ‰) for sessions 1 and 3, and B2203 and B2205 (EMA-P2, $\delta^{18}O$ = 28.9 ± 1.9 ‰, Elemental Microanalysis) for session 2. These reference materials were routinely included across the different analytical sessions to account for instrumental drift and linearity. In addition, the reference material B2213 (Spruce powder, $\delta^{18}O$ = 23.6 ± 0.1 ‰, Elemental Microanalysis) was introduced during session 2 and 3 to monitor the analytical precision and accuracy of the instrument. Analytical uncertainties were calculated following the method described in P. Szpak et al. (2017). The measurement precision specific to standards was estimated to be ± 2 ‰ (degrees of freedom (df) = 37, 1σ). The systematic and random uncertainties were estimated to be ± 2 ‰. The total uncertainty for each sample which accounts for temporal and linear drifts of the standards, the analytical precision and accuracy of the instrument, and the reproducibility of the standards was calculated using a Monte Carlo bootstrap approach. The total amount of oxygen released by the samples was estimated by comparing the thermal conductivity detector (TCD) CO peak area of the samples with the TCD signal of the B2203 reference material (O = 20.87 ± 0.29 wt.%, 1σ). Different amounts of B2203 were weighed out to establish a linear calibration regression covering the entire range of oxygen content observed in the tholins samples (8–45 µg of O). The standard uncertainty for each sample was estimated by propagating the uncertainty in both the slope and y-intercept of the TCD calibration regression, in addition to the weighing uncertainty.

3. OXYGEN INCORPORATION

The total oxygen content (O wt%) has been found to vary significantly from one tholin sample to the other (see Table 2). This Owt% includes the ^{18}O that is incorporated via the ion beam as well as some oxygen contamination (^{16}O and ^{18}O). While no oxygen is present in the initial gas mixture used for synthesis, it is well established that tholins typically exhibit an oxygen content of around 5 wt% (M. L. Cable et al. 2012). However, our measurements show considerably higher values, ranging from 1.8% to 19.4% in the insoluble fraction and 8.4% to 17.2% in the soluble fraction. The exact source of this oxygen contamination remains unclear. The initial fear was that

water condensation at 150 K in the experimental chamber could lead to interactions with the tholins, introducing oxygen. However, our results do not show a clear correlation between sample temperature and oxygen content, as both 150 K and 300 K samples exhibit unusually high O wt% values. Another possible explanation is contamination from an unknown source during the solubilization process. Improving the solubilization protocol and minimizing potential contamination sources could help mitigate this issue. C. D. Neish et al. (2009, 2010) showed that the hydrolysis of tholins in 13 wt% ammonia-water is possible, which opens up the possibility that a similar process is occurring in our tholins in methanol solution (methanolysis). However such contamination will be taken into account in the following calculations. Figure 2 shows a schematic overview of the isotopic oxygen values that have to be calculated in order to determine the amount of oxygen that is incorporated in the tholin samples via irradiation. Here, the total amount of oxygen ($Owt\%$) corresponds to the sum of ^{18}O ($^{18}O_{sample}$) and ^{16}O ($^{16}O_{sample}$). The $^{18}O_{sample}$ includes the ^{18}O that stems from contamination ($^{18}O_{conta}$) and the amount of ^{18}O that is added or incorporated through the irradiation ($^{18}O_{added}$) which is the value we aim to determine.

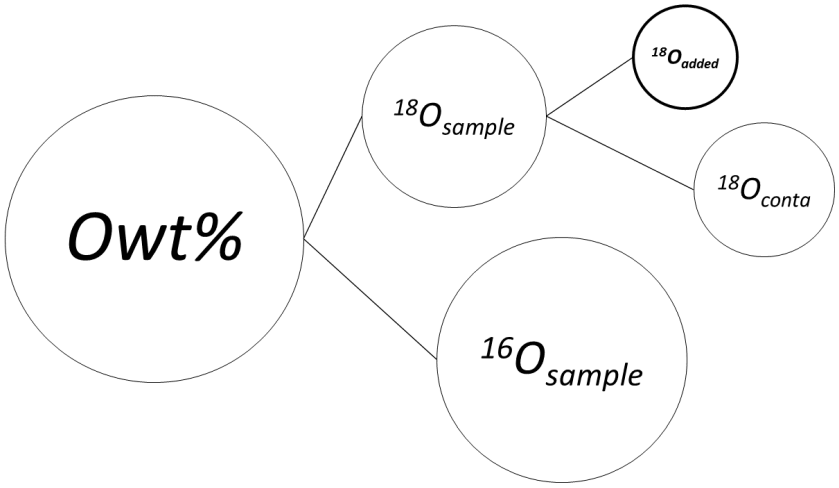

Figure 2. Schematic overview of the calculated amounts of different isotopic oxygen wt%; Circles sizes are not up to scale.

In order to find $^{18}O_{added}$, first, the ^{18}O/^{16}O ratio is calculated with the δ^{18}O gathered from the IRMS measurement. We determine two ratios, one for the total of each sample $(^{18}O/^{16}O)_{sample}$ and one for the contamination $(^{18}O/^{16}O)_{conta}$:

$$\left(\frac{^{18}O}{^{16}O}\right)_{sample} = \left[\left(\frac{\delta^{18}O_{sample}}{1000}\right) + 1\right] * \left(\frac{^{18}O}{^{16}O}\right)_{SMOW} \tag{2}$$

$$\left(\frac{^{18}O}{^{16}O}\right)_{conta} = \left[\left(\frac{\delta^{18}O_{conta}}{1000}\right) + 1\right] * \left(\frac{^{18}O}{^{16}O}\right)_{SMOW} \tag{3}$$

where $SMOW = 1/498.7$. For the ratio of the contamination, $\delta^{18}O$ is the average of all $\delta^{18}O$-values of the non-irradiated and neon-irradiated samples. This average is 15.2 ‰ and 8.3 ‰ for the insoluble and soluble part, respectively. With both ^{18}O/^{16}O ratios of the total sample and the contamination, we can calculate the amount of ^{18}O. In order to convert these atom-based ratios into

Table 2. Results of the IRMS-measurements of the tholin samples: total oxygen wt% (O), δ^{18}O; together with the calculated oxygen isotope ratios for all samples. The δ and σ mark the error for the respective values.

Sample	O (wt.%)				δ^{18}O (‰)				^{18}O/^{16}O$_{\text{total}}$			
	insoluble	δ	soluble	δ	insoluble	σ	soluble	σ	insoluble $\times10^{-3}$	σ $\times10^{-6}$	soluble $\times10^{-3}$	σ $\times10^{-6}$
T0p	10.7	2.1	8.4	2.1	13.7	2.9	13.1	3.2	2.03	3.36	2.03	3.71
T0f	12.9	2.1	8.9	2.1	14.5	3.5	5.9	3.8	2.03	4.05	2.02	4.40
T1	18.7	2.1	16	2.1	41.5	15	30.4	6.2	2.09	17.4	2.07	7.18
T2	3.8	2.1	9.8	2.1	81.7	11.2	39.4	3.9	2.17	13.0	2.08	4.52
T3	17.6	2.1	16	2.1	20.2	5.6	23.5	5.8	2.05	6.48	2.05	6.71
T4	3.4	2.1	9.4	2.1	57.7	7.8	21.7	3.6	2.12	9.03	2.05	4.17
T5	4.5	2.1	9.4	2.1	369.9	57.7	38.7	3.8	2.75	66.8	2.08	4.40
T6	19.4	2.1	17.2	2.1	42.1	23	26.6	7.6	2.09	26.6	2.06	8.80
T7	5.4	2.1	9.2	2.1	99.7	13.3	45.5	3.8	2.21	15.4	2.10	4.40
T8	10.1	2.1	10.4	2.1	110.8	14.8	43.5	4.1	2.23	17.1	2.09	4.75
T9	1.8	2.1	10.4	2.1	16.2	4.4	5.3	3.7	2.04	5.09	2.02	4.28
T10	12.6	2.1	10.8	2.1	17.1	4.5	6.6	4.2	2.04	5.21	2.02	4.86
T11	9.6	2.1	9	2.1	16.1	3.5	9.3	3.3	2.04	4.05	2.02	3.82
T12	4.1	2.1	9.6	2.1	13.7	4.5	9.6	3.9	2.03	5.21	2.02	4.51

weight-based percentages, we take into account the total mass contributed by each isotope, which is $m_{18O} = 17.999$ and $m_{16O} = 15.995$ for ^{18}O and ^{16}O, respectively.

$$^{18}O_{sample} = \frac{\frac{^{18}O}{^{16}O}_{sample} * m_{18O}}{m_{16O} + (\frac{^{18}O}{^{16}O}_{sample} * m_{18O})} * Owt\% \tag{4}$$

$$^{18}O_{conta} = \frac{\frac{^{18}O}{^{16}O}_{conta} * m_{18O}}{m_{16O} + (\frac{^{18}O}{^{16}O}_{conta} * m_{18O})} * Owt\% \tag{5}$$

The amount of ^{18}O added by ion incorporated is simply the difference between $^{18}O_{sample}$ and $^{18}O_{conta}$:

$$^{18}O_{added} = (^{18}O_{sample} - ^{18}O_{conta}) \tag{6}$$

The results from the IRMS measurements ($\delta^{18}O$ & Owt%) together with the calculated isotopic oxygen ratios for all samples are shown in Table 2, while the ^{18}O abundances in ppm can be found in table 3. The isotopic ratios for all samples as well as the added ^{18}O for the oxygen irradiated samples are also shown in figure 3.

The results of the EA-IRMS show the degree of oxygenation of our tholin samples. Figure 3 show the ^{18}O/^{16}O ratios for all tholin samples, divided into non-irradiated, $^{18}O^{q+}$ irradiated and $^{20}Ne^{q+}$ irradiated samples for the insoluble and soluble part. Regarding these values, two distinct

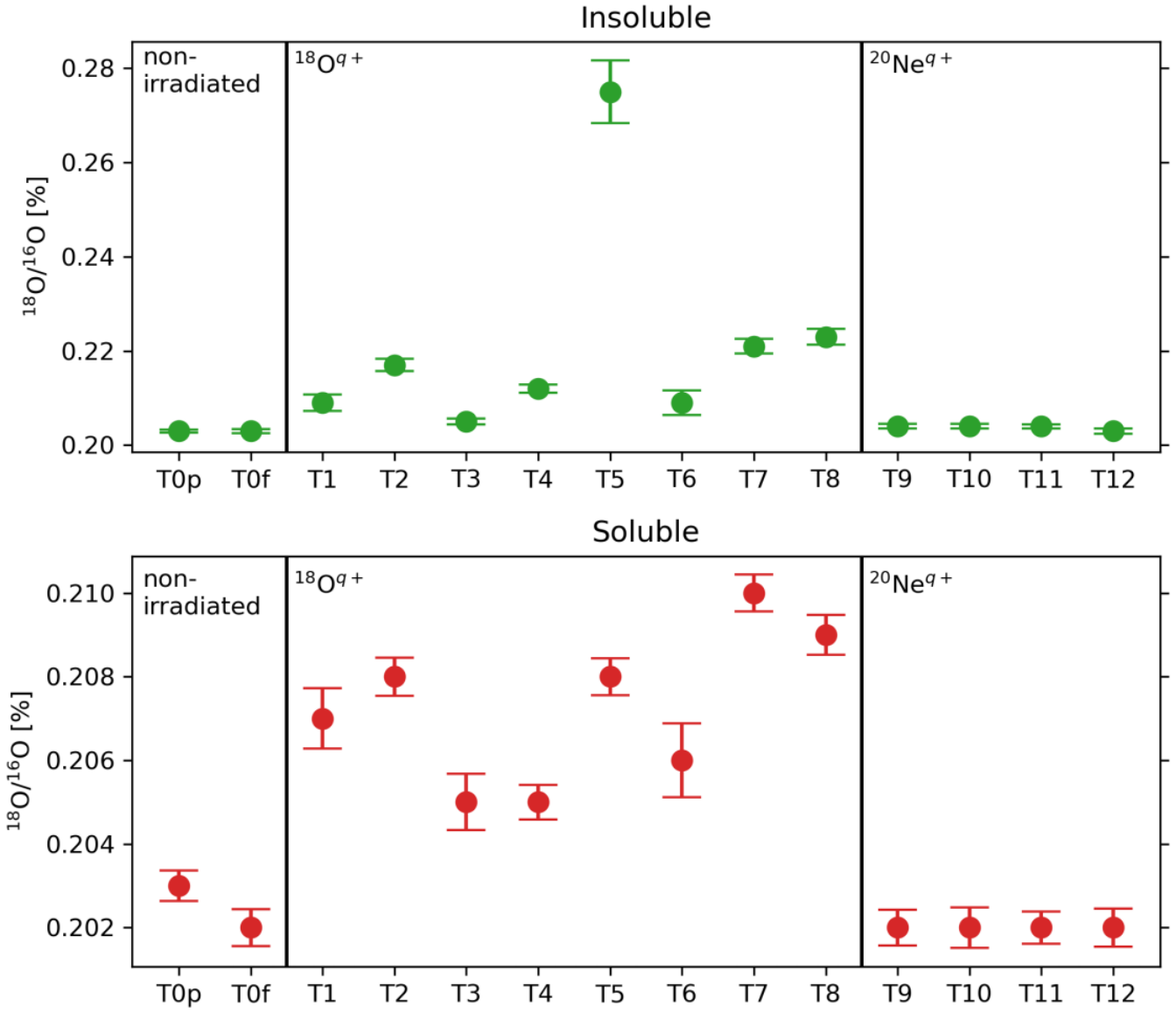

Figure 3. Isotopic oxygen ratios for the insoluble and soluble part of all tholin samples (top and bottom, respectively)

observations can be made. Firstly, the $^{18}O^{q+}$ irradiated samples show higher $^{18}O/^{16}O$ ratios than all other samples with the lowest $^{18}O^{q+}$-irradiated sample T3 at 2.05±0.01 x 10^{-3} and the highest for the $^{20}Ne^{q+}$-irradiated sample T9 at 2.04±0.01 x 10^{-3}. All samples irradiated with oxygen ions fall above T3, while all other samples, non-irradiated and neon-irradiated fall below T9. This general difference in $^{18}O/^{16}O$ between non-irradiated and $^{20}Ne^{q+}$ irradiated compared to $^{18}O^{q+}$ irradiated samples implies that oxygen incorporation is possible through ion irradiation. Secondly, there is a substantial difference in the $^{18}O/^{16}O$ values of the insoluble and soluble part of the tholins. The $^{18}O/^{16}O$ ratios of the insoluble part exceeds the soluble part in most samples, exception being the sample T3 which posses overlapping uncertainties.

Apart from the isotopic oxygen ratios, the calculated $^{18}O_{added}$ quantifies the amount of the tholin sample that consists of ^{18}O which has been added by the irradiation. When viewing these results

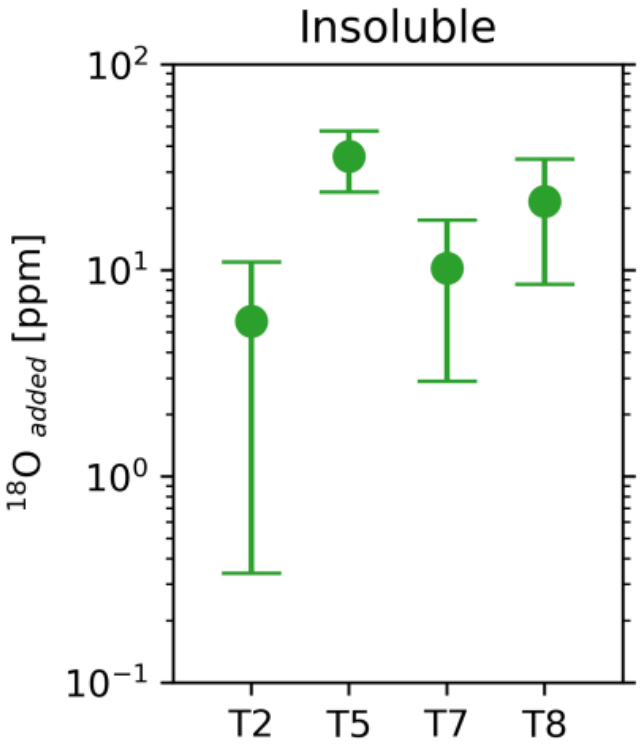

Figure 4. The amount of ^{18}O added to the oxygen irradiated samples T2, T5, T7 and T8 through incorporation

in Table 3, two key observations can be made. First, the $^{18}O_{added}$ values are significantly smaller compared to the ^{18}O from contamination , with the contamination exceeding the amount of added ^{18}O by a factor of ∼201 in the extreme case of T3. The smallest ratio is observed in sample T5, where the factor is ∼3. All soluble samples and the insoluble samples T1, T3, T4 and T6 , exhibit uncertainties that exceed the corresponding measured values, making them unreliable. This is attributed to a high level of contamination combined with the relatively small amount of added oxygen, further compounded by the propagation of uncertainties through the multiple intermediate calculations required to determine $^{18}O_{added}$. Therefore, Figure 4, only shows the added oxygen for the insoluble part of the samples T2, T5, T7 and T8 with 6±5, 36±12, 10±7 and 22±13 ppm, respectively, where the uncertainties to not surpass the value.

Overall, the results suggest that the incorporation of oxygen ions is more effective in the insoluble part of tholins. Several mechanisms could account for this phenomenon. The insoluble part of tholins contains more unsaturated bonds (Á. Somogyi et al. 2012; J. Maillard et al. 2018). This, along with a greater number of larger molecules in the insoluble fraction, results in an increased number of reactive sites and more opportunities for oxygen ions to bind. F. Schulz et al. (2021) reports that the molecules in the insoluble part are generally highly conjugated in comparison to the soluble part. This adds another favorable property for oxygen incorporation as highly conjugated systems posses delocalized electrons that create a localized electron density increase, attracting oxygen. Apart from the chemical binding, oxygen ions could also be caught electrostatically, via physical adsorption or plainly being physically trapped inside bulky macromolecules. However, it is unlikely that these types

Table 3. Abundances of ^{18}O in the samples; divided into the total amount of ^{18}O ($^{18}O_{total}$), the ^{18}O that comes from the oxygen contamination of the sample ($^{18}O_{conta}$) and the ^{18}O that is added to the sample through the ion irradiation ($^{18}O_{added}$).

Sample	$^{18}O_{total}$ (ppm)				$^{18}O_{conta}$ (ppm)				$^{18}O_{added}$ (ppm)			
	insoluble	σ	soluble	σ	insoluble	σ	soluble	σ	insoluble	σ	soluble	σ
T0p	244	28	192	28	245	31	191	48				
T0f	295	28	202	27	295	32	202	50				
T1	438	29	371	28	427	36	363	79	11	24	8	75
T2	93	30	229	28	87	28	222	54	6	5	7	46
T3	404	28	369	28	402	35	363	79	2	22	5	75
T4	81	29	216	28	78	28	213	52	3	5	3	44
T5	139	38	220	28	103	28	213	52	36	12	6	44
T6	455	29	398	28	443	37	390	85	12	25	7	80
T7	134	30	217	29	123	29	209	51	10	7	8	43
T8	253	30	244	28	231	30	236	56	22	13	8	49
T9	41	28	235	27	41	28	236	56				
T10	289	28	245	27	288	32	245	57				
T11	220	28	205	28	219	30	204	50				
T12	94	28	218	28	94	28	218	53				

of binding would persist over extended periods, especially considering that the samples are stored in solvent for a prolonged time.

Due to the limited number of data points available for each experimental parameter, we are unable to reliably assess the individual dependencies of these parameters on the measured $^{18}O_{added}$ values. As a consequence, it becomes challenging to discern clear dependencies among the individual parameters. These experiments should therefore be regarded primarily as proof-of-concept studies and we refrain from drawing definitive conclusions regarding such parameter dependencies. For the purpose of this analysis, we therefore assume that neither the ion beam energy, fluence nor the sample temperature significantly influence the $^{18}O_{added}$ values under the given experimental conditions. In order to further investigate the behavior of oxygen ion incorporation with varying experimental parameters and to better understand the differing responses of soluble and insoluble fractions, a larger dataset is required. Additional experiments, varying only one of the experimental parameters while not changing the others, will be necessary.

4. IMPLICATIONS FOR TITAN AEROSOLS AND THEIR ANALOGS

The incorporation of oxygen ions into tholins carries significant implications for the oxygen chemistry in Titan's atmosphere. Previous tholin synthesis experiments confirmed that the presence of CO in the initial gas-mixture leads to the formation of astrobiologically interesting molecules like cytosine, uracil, thymine, guanine, glycine and alanine (S. Hörst et al. 2012). Our results demonstrate that oxygen ions, when introduced through irradiation, can be incorporated into the complex organic

molecules, potentially leading to the formation of oxygenated functional groups. This process may provide an alternative pathway for the incorporation of oxygen into Titan's aerosols. Furthermore, the presence of oxygenated compounds, even in trace amounts, could also have astrobiological implications for Titan, as they might facilitate the formation of compounds indispensable for life that precipitate to Titan's surface.

Understanding how many oxygen ions get incorporated helps to quantify the degree of chemical modification that Titan's aerosols might undergo. If a significant fraction of incident ions are incorporated, it suggests that this particular ion-driven process is a viable mechanism for introducing oxygen into Titan's organic haze layers. This would impact modeling efforts regarding the chemistry in Titan's atmosphere by providing an additional pathway to forming oxygenated molecules. In order to estimate the amount of ions incorporated into the tholins, we can calculate the mass added to the sample by the ion beam. The calculations begins by determining the mass of the added oxygen of the thin film sample. Here, we assume the mass of the sample to be that of a cylinder with a radius of 1 $\pm$ 0.01 cm, a thickness of 500$\pm$50 nm and a density of 1.33 $\pm$ 0.05 g cm^{-3} (derived from H. Imanaka et al. (2012) and C. He et al. (2017)). The mass of the cylinder is then multiplied by the share of added oxygen in the tholins $^{18}O_{added}$ of each sample. This mass then is divided by the mass of an ^{18}O-ion (2.99 $\times$ 10^{-26} kg) to get an approximate number of ions that have been added to the sample. Dividing the number of incorporated ions by the total fluence delivers the share of the ion beam.

Naturally, this calculation comes with several assumptions. First, we assume an error of 30% for the fluence as the beam was misaligned (see figure 1). Second, we consider the thickness of the thin-film to be constant, although the thickness decreases as material sputters away. In order to mitigate this issue, we make additional calculations for 250 $\pm$ 50 nm. Third, we assume a constant density of the tholins. However, previous experiment irradiating astrophysical ice analogs, demonstrate that a sample tends to compress during irradiation, not only decreasing the thickness but also increasing the density (E. Dartois et al. 2013; C. Mejía et al. 2015; P. Boduch et al. 2015). Finally, calculations are only performed for the insoluble fractions of T2, T5, T7 and T8, as the uncertainties of $^{18}O_{added}$ for the other samples were too great to calculate reliable shares. The ion beam shares presented here only represent the insoluble part, which accounts for approximately 65% of the tholins (J. Maillard et al. 2018). All of these assumptions have to be taken into a account as possible sources of biases.

The results of the share calculation can be seen in Figure 5. Shares were calculated for each sample with the two different thicknesses in order to account for sputtering. The share of ions being incorporated into each sample varies between 2 $\pm$ 1 % and 16 $\pm$ 6 % depending on sample and its thickness. A comparison of the samples indicates that the total fluence of ion irradiation does not significantly affect the overall fraction of ions being incorporated. For instance, T5 was irradiated with four times the amount of ions than T2, T7 and T8 and lies in between those samples.

From these results, we can infer that oxygen ions have a $\sim$2-16% probability of incorporating into an aerosol in Titan's atmosphere. This range reflects lower limits at which incorporation could happen. We suspect that solubilizing and storing our samples in methanol might lead to an isotopic exchange between our samples and the solvent. Such exchange of oxygen isotopes has been observed before, however on oligosaccharides dissolved in methanol and not tholins (S. Ollivier et al. 2021). It is therefore possible that the amount of oxygen ion incorporation is even higher than measured here.

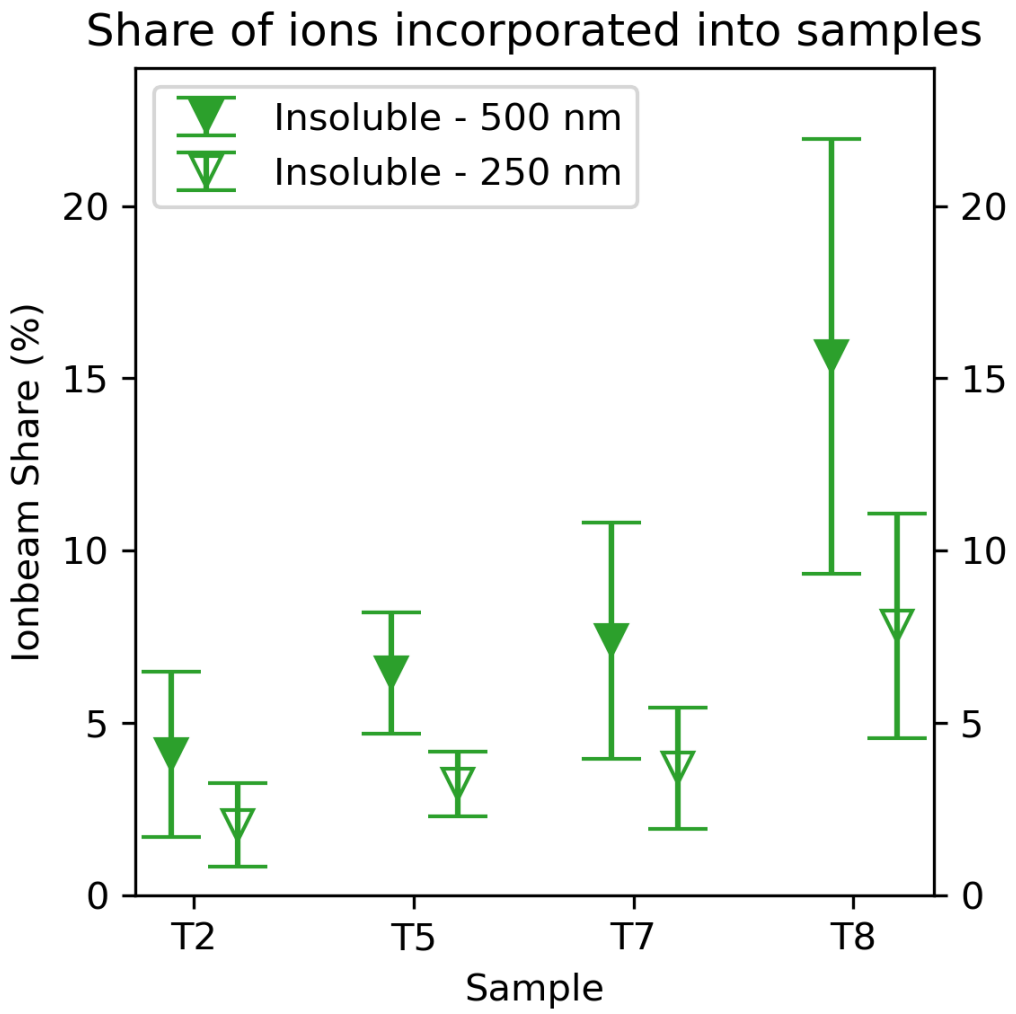

Figure 5. Shares of ions being incorporated into the tholin thin-film samples T2, T5, T7 and T8; for the insoluble part with a thickness of 250 and 500 nm

Future experiments that circumvent this solubilization and use solid sample instead will show the extent to which isotopic exchange between sample and solvent occurs.

Our findings provide crucial input for refining models of ion interactions with Titan's aerosols. By utilizing the incorporation probabilities derived from our experiments, models can simulate the fate of oxygen ions in Titan's atmosphere more accurately. Additionally, the lack of correlation between fluence and incorporation probability suggests that models should treat oxygen ion incorporation as a probabilistic event rather than a cumulative effect. This improved understanding will enhance predictions of oxygen incorporation into Titan's organic aerosols. The precipitation through Titan's atmosphere and final sedimentation of oxygenated organic molecules may play a significant role in shaping the surface chemistry of Titan, potentially contributing to the formation of complex materials with astrobiological significance.

5. SUMMARY AND CONCLUSION

In this study, tholin thin-film samples have been irradiated with either $^{18}O^{q+}$ or $^{20}Ne^{q+}$ ions at different energies (35 and 70 keV), temperatures (150 and 300 K) and fluences (0.6 - 4 $\times$ 10^{15} ions.cm^{-2}). Ex-situ EA-IRMS measurements determined the $\delta^{18}O$ values of the soluble and insoluble part of the samples. In order to investigate the degree of oxygenation and answer the question of wether oxygen incorporation through irradiation is possible, calculations of oxygen isotope ratios were performed. The following conclusions can be made:

1. The oxygen isotope analysis demonstrates elevated $^{18}O/^{16}O$ for all samples being irradiated with O-ions, as opposed to the non- and Ne-irradiated samples. This shows that oxygen incorporation into tholins through irradiation is certain, having implications on the incorporation of oxygen into the complex organic molecules in Titan's aerosols.

2. The amount of incorporated ^{18}O ranges from 6$\pm$5 to 36$\pm$12 ppm.

3. The elevated amount of ^{18}O in the insoluble part of the tholins compared to the soluble indicate that oxygen c is more effective in the more unsaturated, highly conjugated and over all more complex molecules found in the insoluble part.

4. The total share of oxygen ions from the ion beam being incorporated into the tholins amounts to $\sim$2-16% depending on the sample, its thickness.

Overall, these analog experiments have significant implications for the incorporation of energetic oxygen into the aerosols in Titan's atmosphere. While we demonstrated that incorporation is possible, the ultimate destination in terms of chemical bindings is still an open question. Future experiments focusing on the chemical analysis and identification of specific oxygenated molecules will shed light on this issue.

ACKNOWLEDGMENTS

We thank the Programme National de Planétologie (PNP) and the French National Research Agency in the framework of the "Investissements d'avenir" program (ANR-15-IDEX-02) and the generic call for proposals (ANR-22-CE49- 0017) for supporting this work. The experiments were performed at the ARIBE platform of the Grand Accélérateur National d'Ions Lourds (GANIL) by means of the CIRIL Interdisciplinary Platform, part of CIMAP laboratory, Caen, France. We thank the staff of CIMAP-CIRIL and GANIL for their invaluable support. In particular, we thank Patrick Rousseau and Claire Feierstein for the ion beam preparation. We acknowledge the funding from ANR IGLIAS grant ANR-13-BS05-0004 of the French Agence Nationale de la Recherche. A CC-BY public copyright license has been applied by the authors to the present document and will be applied to all subsequent versions up to the Author Accepted Manuscript arising from this submission, in accordance with the ANR grants' open access conditions.

AUTHOR CONTRIBUTIONS

FM was responsible for execution of the experiments, data-analysis, writing and submission of the manuscript. VV came up with the initial research concept and obtained the funding. LV, LF and LB were responsible for the IRMS analysis, with LV processing the subsequent data from said analysis.

PB, AD and HR lead the irradiation experiments, while SH, CP and CH were responsible for the sample synthesis. All authors were involved in the editing process.

REFERENCES

Augé, B., Been, T., Boduch, P., et al. 2018, Review of Scientific Instruments, 89, 075105, doi: 10.1063/1.5028056

Boduch, P., Brunetto, R., Ding, J., et al. 2016, Icarus, 277, 424

Boduch, P., Dartois, E., de Barros, A. L., et al. 2015, in , IOP Publishing, 012008

Cable, M. L., Hörst, S. M., Hodyss, R., et al. 2012, Chemical Reviews, 112, 1882, doi: 10.1021/cr200221x

Crary, F. J., Magee, B. A., Mandt, K., et al. 2009, Planetary and Space Science, 57, 1847, doi: 10.1016/j.pss.2009.09.006

Cravens, T. E., Robertson, I. P., Ledvina, S. A., et al. 2008, Geophysical Research Letters, 35, doi: 10.1029/2007GL032451

Dartois, E., Ding, J., De Barros, A., et al. 2013, Astronomy & Astrophysics, 557, A97

Ding, J., Boduch, P., Domaracka, A., et al. 2013, Icarus, 226, 860

Hartle, R. E., Sittler, E. C., Neubauer, F. M., et al. 2006a, Planetary and Space Science, 54, 1211, doi: 10.1016/j.pss.2006.05.029

Hartle, R. E., Sittler Jr., E. C., Neubauer, F. M., et al. 2006b, Geophysical Research Letters, 33, doi: 10.1029/2005GL024817

Haythornthwaite, R. P., Coates, A. J., Jones, G. H., et al. 2021, The Planetary Science Journal, 2, 26, doi: 10.3847/PSJ/abd404

He, C., Hörst, S. M., Riemer, S., et al. 2017, The Astrophysical Journal, 841, L31, doi: 10.3847/2041-8213/aa74cc

He, C., Serigano, J., Horst, S., Radke, M., & Sebree, J. 2022, 54, 402.04. https://ui.adsabs.harvard.edu/abs/2022DPS....5440204H

Hörst, S., Yelle, R., Buch, A., et al. 2012, Astrobiology, 12, 809, doi: 10.1089/ast.2011.0623

Hörst, S. M. 2017, Journal of Geophysical Research: Planets, 122, 432, doi: 10.1002/2016JE005240

Hörst, S. M., Vuitton, V., & Yelle, R. V. 2008, Journal of Geophysical Research: Planets, 113, doi: 10.1029/2008JE003135

Imanaka, H., Cruikshank, D. P., Khare, B. N., & McKay, C. P. 2012, Icarus, 218, 247

Johnson, R., Liu, M., & Sittler Jr, E. 2005, Geophysical research letters, 32

Jovanovic, L. 2021, PhD thesis, Université Paris-Saclay

Lavvas, P., Yelle, R. V., Koskinen, T., et al. 2013, Proceedings of the National Academy of Sciences, 110, 2729, doi: 10.1073/pnas.1217059110

Lv, X., Boduch, P., Ding, J., et al. 2014, Monthly Notices of the Royal Astronomical Society, 438, 922

López-Puertas, M., Dinelli, B. M., Adriani, A., et al. 2013, The Astrophysical Journal, 770, 132, doi: 10.1088/0004-637X/770/2/132

Maillard, J., Carrasco, N., Schmitz-Afonso, I., Gautier, T., & Afonso, C. 2018, Earth and Planetary Science Letters, 495, 185, doi: 10.1016/j.epsl.2018.05.014

Mejía, C., De Barros, A., Duarte, E. S., et al. 2015, Icarus, 250, 222

Mifsud, D. V., Kaňuchová, Z., Herczku, P., et al. 2024, Icarus, 411, 115926

Neish, C. D., Somogyi, Á., Lunine, J. I., & Smith, M. A. 2009, Icarus, 201, 412

Neish, C. D., Somogyi, , & Smith, M. A. 2010, Astrobiology, 10, 337, doi: 10.1089/ast.2009.0402

Ollivier, S., Tarquis, L., Fanuel, M., et al. 2021, Analytical Chemistry, 93, 6254

Ruf, A., Bouquet, A., Boduch, P., et al. 2019, The Astrophysical journal letters, 885, L40

Schulz, F., Maillard, J., Kaiser, K., et al. 2021, The Astrophysical Journal Letters, 908, L13, doi: 10.3847/2041-8213/abd93e

Sittler, E. C., Cooper, J. F., Sturner, S. J., & Ali, A. 2020, Icarus, 344, 113246, doi: 10.1016/j.icarus.2019.03.023

Sittler Jr, E., Ali, A., Cooper, J., et al. 2009, Planetary and Space Science, 57, 1547

Sittler Jr, E., Johnson, R., Smith, H., et al. 2006, Journal of Geophysical Research: Space Physics, 111

Snowden, D., Smith, M., Jimson, T., & Higgins, A. 2018, Icarus, 305, 186, doi: 10.1016/j.icarus.2018.01.014

Somogyi, Á., Smith, M. A., Vuitton, V., Thissen, R., & Komáromi, I. 2012, International Journal of Mass Spectrometry, 316, 157

Strazzulla, G., Baratta, G., Leto, G., & Gomis, O. 2007, Icarus, 192, 623

Szpak, P., Metcalfe, J. Z., & Macdonald, R. A. 2017, Journal of Archaeological Science: Reports, 13, 609

Waite, J. H., Young, D. T., Cravens, T. E., et al. 2007, Science, 316, 870, doi: 10.1126/science.1139727

Xu, G., Hibino, Y., Suzuki, Y., et al. 2000, Colloids and Surfaces B: Biointerfaces, 19, 237

Ziegler, J. F., Ziegler, M. D., & Biersack, J. P. 2010, Nuclear Instruments and Methods in Physics Research Section B: Beam Interactions with Materials and Atoms, 268, 1818